nature materials

SUPPLEMENTARY INFORMATION
https://doi.org/10.1038/s41563-017-0003-3

In the format provided by the authors and unedited.

Designing perturbative metamaterials from discrete models

Kathryn H. Matlack[1,2], Marc Serra-Garcia[1*], Antonio Palermo[3], Sebastian D. Huber[2] and Chiara Daraio[1,4]

[1]Department of Mechanical and Process Engineering, ETH Zürich, Zürich, Switzerland. [2]Institute for Theoretical Physics, ETH Zürich, Zürich, Switzerland. [3]Department of Civil, Chemical, Environmental and Materials Engineering – DICAM, University of Bologna, Bologna, Italy. [4]California Institute of Technology, Pasadena, California, USA. Kathryn H. Matlack and Marc Serra Garcia contributed equally to this work. *e-mail: sermarc@ethz.ch

Designing Perturbative Metamaterials from Discrete Models

Kathryn H. Matlack*[1,3], Marc Serra Garcia*[1a], Antonio Palermo[2], Sebastian D. Huber[3], Chiara Daraio[1,4]

[1]Department of Mechanical and Process Engineering, ETH Zürich, Zürich, Switzerland

[2]Department of Civil, Chemical, Environmental and Materials Engineering - DICAM, University of Bologna, Bologna, Italy

[3]Institute for Theoretical Physics, ETH Zürich, Zürich, Switzerland

[4]California Institute of Technology, Pasadena, CA

*These authors contributed equally to this work

a) sermarc@ethz.ch

Supplementary Information

SI1. Calculation of the Schrieffer-Wolff transformation as a series expansion

We create a reduced order model for an infinite, periodic perturbative metamaterial by calculating a Schrieffer-Wolff transformation of the perturbation matrix V_{ij}. The Schrieffer-Wolff transformation is calculated as a series expansion up to order n. We refer to the resulting reduced matrix as V^R. We will also use H_0^R to refer to the unperturbed cells' dynamic matrix, restricted to the subspace of modes that lie in the frequency range of interest. The reduced matrices V^R and H_0^R describe the force acting on an arbitrary unit cell (we call it the center) as a function of the displacement of its neighbors. When calculating the SW transformation for order n, we must take into account interactions with neighbors that are up to n unit cells away from the center. Figure S1 shows the system under consideration.

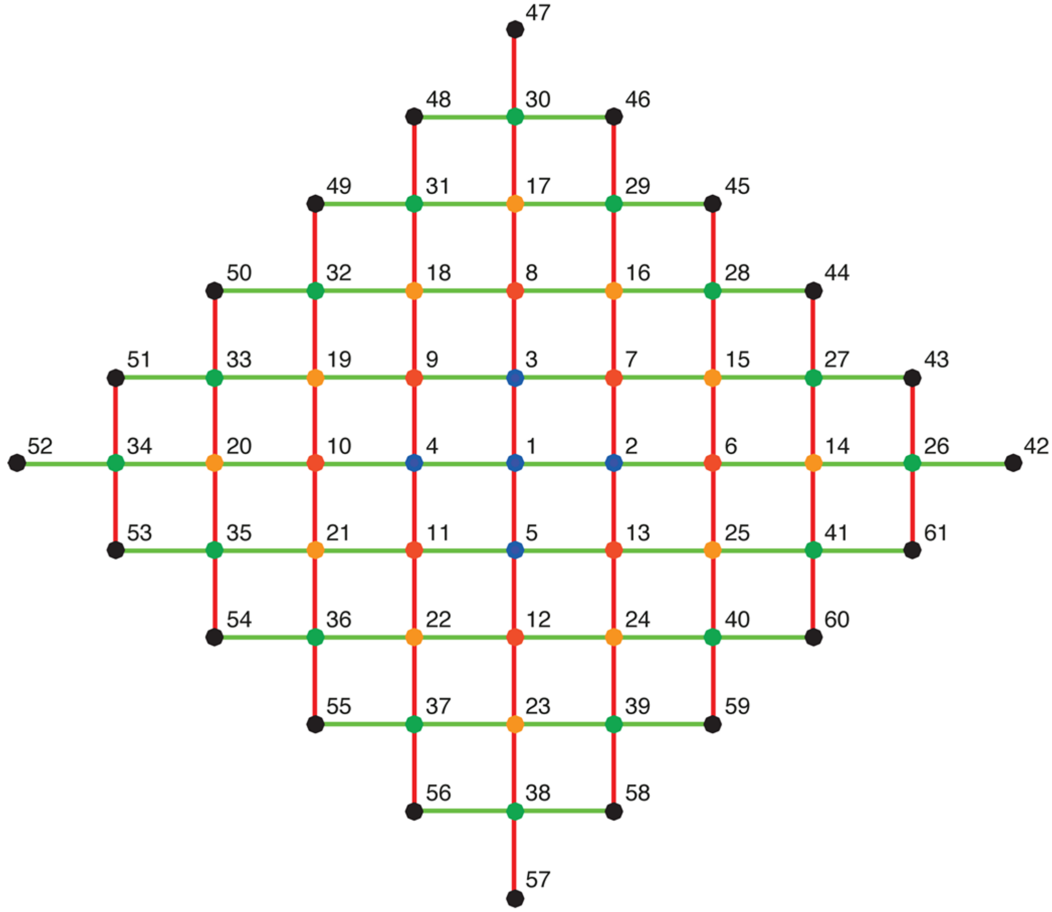

Figure S1 | Test system for the calculation of the Schrieffer-Wolff transformation. The dots represent unit cells. For a first order calculation, only the blue dots are required. We then add the black dots (for second order), green dots (for third order), yellow dots (for fourth order) and red dots (for fifth order). The lines represent the coupling between a unit cell and its nearest neighbor in the x-direction (V^H, green) and y-direction (V^V, red).

We first proceed to assemble the matrices V and H_0 for the coupled system represented in Fig. S1. These are $m \times m$ square matrices, where $m = l \times (number\ of\ cells)$, l being the number of local modes per unit cell. The number of local modes l refers to the full description obtained from finite elements (as described in the coupling matrix extraction part of the methods section), containing 40 modes per plate for cases described in our paper, and not to the final reduced model which contains 1-6 modes per unit cell.

The matrix assembly utilizes the matrices V^H(Describing the effect of the beams coupling horizontal plates), V^V (Describing the effect of the beams coupling vertical plates), V^{HOLE} (Describing the effect of the holes) and H_0^S (Describing the unperturbed modes of a single plate). For unit cells containing multiple plates, additional matrices should be included to account for inter-plate couplings inside the unit cell. The matrices V^H and V^V are obtained by simulation of a two-plate system as described in the Coupling Matrix Extraction part of the Methods section. The horizontal two-plate simulation yields the coupling V^{LR} between horizontally neighboring plates. In addition, the plate on the left experiences a frequency shift V_{LL} due to having beams on the right, and the plate on the right experiences a shift V_{RR} due to having beams on the left. We obtain an analogous result for a system of vertical plates, with local frequency shifts given by V^{DD} and

V^{UU}, and an inter-plate coupling given by V^{DU}. The matrices V^{H} and V^{V}, which summarize the effect of all 4 nearest neighbors, are structured as:

$$V^{H} = \begin{pmatrix} V^{LL} & V^{LR} \\ V^{RL} & V^{RR} \end{pmatrix} \qquad\qquad V^{V} = \begin{pmatrix} V^{DD} & V^{DU} \\ V^{UD} & V^{UU} \end{pmatrix}$$

Where the terms V^{LL}, V^{RR}, V^{UU} and V^{DD} represent local changes in the unit cell dynamics brought by the beams placed on the right, left, bottom and top of the plate respectively, and V^{LR}, V^{RL}, V^{UD}, V^{DU} represent the inter-plate couplings from the beams. The terms V^{LL}, V^{RR}, V^{UU} and V^{DD} are what we correct for with the introduction of holes in the plate. For a given unit cell number r, the matrix V describing the whole system in Fig. S1 satisfies:

$$V_{i+(r-1)l,j+(r-1)l} = V_{ij}^{LL} + V_{ij}^{RR} + V_{ij}^{DD} + V_{ij}^{UU} + V_{ij}^{HOLE}$$

For a pair of adjacent unit cells r and t, with r being on the left of t, we have $(1 \leq i,j \leq l)$:

$$V_{i+(r-1)l,j+(t-1)l} = V_{ij}^{LR}$$
$$V_{i+(t-1)l,j+(r-1)l} = V_{ij}^{RL}$$

For a pair of adjacent unit cells r and t, with r below t, we have $(1 \leq i,j \leq l)$:

$$V_{i+(r-1)l,j+(t-1)l} = V_{ij}^{DU}$$
$$V_{i+(t-1)l,j+(r-1)l} = V_{ij}^{UD}$$

The term H_0 is the diagonalized, unperturbed (excluding effects of the beams and holes) dynamical matrix of the system depicted in Fig. S1, contains as many diagonal copies of H_0^S as unit cells required for the desired order of approximation, and has the form:

$$H_0 = \begin{pmatrix} H_0^S & 0 & \dots & 0 \\ 0 & H_0^S & \dots & 0 \\ \dots & \dots & \dots & \dots \\ 0 & 0 & \dots & H_0^S \end{pmatrix}$$

After assembling the matrices, we proceed to compute the Schrieffer-Wolff transformation as a series expansion of order $n \leq 5$. The new effective dynamical matrix will be given by:

$$H_{eff}^{R} = H_0^{R} + V^{R} = \wp^{T} \left[H_0 + \sum_{r=1}^{n} H_i \right] \wp$$

Where $\wp$ represents a projector into the subspace of relevant modes. As a consequence of this projection, the resulting system H_{eff}^{R} involves only the relevant modes. The first five terms H_i in the series expansion of the Schrieffer-Wolff transformation are given by[18]:

$$
\begin{aligned}
H_1 &= V \\
H_2 &= (1/2)[S_1, \mathcal{O}(V)] \\
H_3 &= (1/2)[S_2, \mathcal{O}(V)] \\
H_4 &= (1/2)[S_3, \mathcal{O}(V)] - (1/24)\big[S_1, \big[S_1, [S_1, \mathcal{O}(V)]\big]\,\big] \\
H_5 &= (1/2)[S_4, \mathcal{O}(V)] \\
&\quad - (1/24)\Big(\big[S_2, \big[S_1, [S_1, \mathcal{O}(V)]\big]\,\big] + \big[S_1, \big[S_2, [S_1, \mathcal{O}(V)]\big]\,\big] + \big[S_1, \big[S_1, [S_2, \mathcal{O}(V)]\big]\,\big]\Big)
\end{aligned}
$$

Where $\mathcal{O}(V)$ is a square matrix with the same size of V, but containing only block-off-diagonal terms, i.e. those that couple a relevant mode to an irrelevant mode, and having all the block-diagonal terms set to zero. The symbol $[A, B]$ represents a commutator: $[A, B] = AB - BA$. The terms S_1 to S_4 are given by:

$$
\begin{aligned}
S_1 &= \mathcal{L}(V) \\
S_2 &= -\mathcal{L}([\mathcal{D}(V), S_1]) \\
S_3 &= \mathcal{L}\big(-[\mathcal{D}(V), S_2] + (1/3)\big[S_1, [S_1, \mathcal{O}(V)]\big]\big) \\
S_4 &= \mathcal{L}\Big(-[\mathcal{D}(V), S_3] + (1/3)\big(\big[S_1, [S_2, \mathcal{O}(V)]\big] + \big[S_2, [S_1, \mathcal{O}(V)]\big]\big)\Big)
\end{aligned}
$$

Here, $\mathcal{D}(V)$ is a matrix the same size as V but with zeroes replacing all the terms coupling relevant-to-relevant or irrelevant-to-irrelevant modes. The function $\mathcal{L}$ is defined as:

$$
[\mathcal{L}(A)]_{ij} = \begin{cases} \dfrac{A_{ij}}{(H_0)_{ii} - (H_0)_{jj}} & if\ (i, j)\ is\ block - off - diagonal \\ 0 & if\ (i, j)\ is\ block - diagonal \end{cases}
$$

The series expansion of the Schrieffer-Wolff transformation allows us to combine independently-calculated geometric perturbations into reduced-order models that describe the metamaterial's response. Fig. S2 illustrates the accuracy of this process for the paradigmatic example of a system of steel plates coupled through polymer beams (Fig. S2a). This is accomplished by simulating the effect of each perturbation separately (Fig S2b) on a large space of 40 local modes, and then performing a Schrieffer-Wolff transformation to obtain an effective theory that contains only two degrees of freedom per site, corresponding to the two local plate modes (Fig S2c) in the frequency region of interest (Fig S2d).

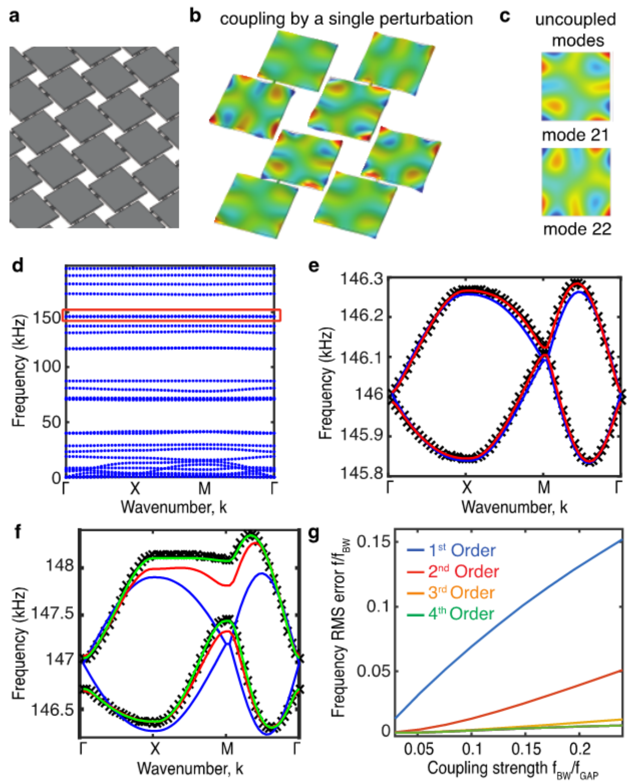

Figure S2 | Method of extracting a reduced-order model. a. Periodic perturbative metamaterial consisting of 10 mm x 10 mm x 0.5 mm steel plates coupled through polymer beams. **b.** Simulation of a two plate system containing a single geometric feature (e.g. beam) used to determine the perturbation introduced by the geometric feature under consideration. **c.** Degenerate plate modes in the frequency region of interest (between 145-149 KHz). **d.** Dispersion relation of a periodic metamaterial highlighting the frequency range of interest. **e.** Comparison between the metamaterial's dispersion relation computed by finite element simulation under Bloch boundary conditions (x) and computed from reduced-order models obtained truncating the Schrieffer-Wolff transformation to first and second order (blue and red respectively) for a metamaterial with a beam stiffness of 4 GPa. **f.** Comparison between finite element simulation (x) under Bloch boundary conditions and reduced-order models truncated at first, second, third and fourth orders (Blue, red, yellow and green respectively). **g.** Relative error of the predicted dispersion relation, as a function of the coupling strength, quantified as the ratio between the bandwidth and the spectral gap to the nearest local mode.

For low perturbation strengths, corresponding to soft beams with a stiffness of 4 GPa, truncating the series expansion to first order produces a satisfactory approximation (Fig S2e). This corresponds to a regime where the perturbations are additive and long-range couplings are negligible, and therefore is optimal for metamaterial design. In contrast, when the perturbation strength is increased by increasing the coupling stiffness to 20 GPa, a fourth-order approximation is required in order to obtain a good agreement between effective theory and metamaterial behavior (Fig S2f), due to nonlinear interactions between geometric elements and due to the increased relative importance of long-range couplings. We observe that the model error (computed as the RMS error between the first order reduced model prediction and the dispersion relation obtained by full finite-element simulation of a periodic system) increases proportionally to the ratio between the coupling strength (measured by the bandwidth) and the gap to the nearest mode (Fig S2g) as predicted by the series expansion of the Schrieffer-Wolff transformation.

The analysis of higher orders of the SW transformation allows us to assess the validity of the weak coupling assumption in the metamaterial design. Large higher-order contributions introduce a dependence between individual design changes, and result in undesired long-range interactions that are hard to remove by altering the material geometry. This indicates that either the coupling V_{ij} introduced by the beams should be reduced, or the spectral gaps $E_i - E_j$ to neighboring local modes should be increased by either modifying the unit cell geometry or selecting different mode(s) (see Supplementary Information).

SI2. Additive Properties of Perturbative Metamaterials

The technique we presented in this paper allows us to design metamaterials based on complex mass-spring models, such as those with nontrivial topological properties. This ability to implement advanced functionality arises from the linear relation between the reduced order model and the metamaterial geometry, which is valid when the Schrieffer-Wolff transformation is evaluated to first order. A linear relation between material and model means that the springs in a mass-spring model corresponding to a system containing multiple inter-plate coupling beams will be the sum of the springs in the mass-spring models corresponding to systems containing each one of the beams (Fig. S3a).

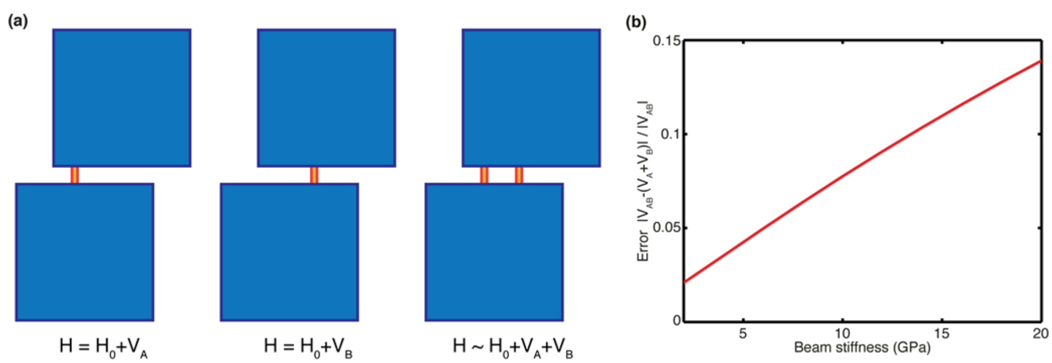

Figure S3 | Beam width linearity. a. Two-plate system used to test the linear dependence between beam width and coupling matrix. **b.** Error in the coupling matrix of a two-beam system obtained by adding single-beam solutions, as a function of the beam stiffness. Higher beam stiffness result in higher relative errors since the first-order Schrieffer-Wolff transformation becomes inaccurate at high coupling strengths.

This linear approximation is valid as long as the first-order perturbative Schrieffer-Wolff transformation is accurate (Fig. S3b). For the polymer beams that we use in this work ($E = 4.02$ GPa), the error in the stiffness matrix is below 5%. This low error allows us to evaluate vast design spaces (exceeding 10^{40} configurations for the beam locations and widths) without having to perform a full finite-element simulation for each design.

Additionally, in the range of beam widths present in our design, the coupling matrix V (which describes the effect of the polymer beams) increases linearly with each beam's width w: $V \approx V_0 \left(\frac{w}{w_0}\right)$, where V_0 and w_0 are the coupling matrix and beam width for a reference configuration. This approximation is very accurate (Fig S4a-c), with an error below 1.2% for the beam widths considered in this work.

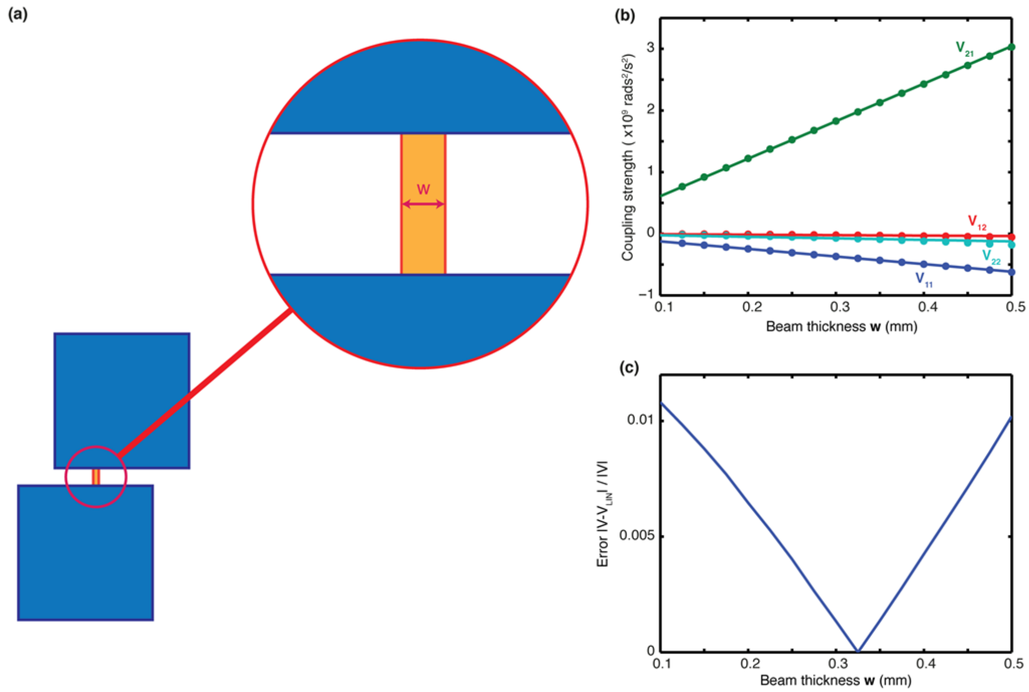

Figure S4 | Beam width linearity. a. Two-plate system used to test the linear relation between beam width and coupling matrix. **b.** Elements of the coupling matrix V_{ij}, describing the coupling between plate modes 21 and 22. The coupling matrices have been obtained by finite element simulation (dots) and by linear extrapolation from a single beam width (solid lines). **c.** Relative error of the coupling matrix as a function of the beam width. The result is exact when the beam width matches the reference width w_0.

The linear relation between beam width and geometry allows us to speed-up the optimization process by simulating a single beam width at every location, and extrapolating the coupling strength of different widths from this single finite element simulation.

SI3. Coupled optimization in the Zero Group Velocity lattice model

Our method for designing metamaterials by separately tuning the design parameters considers only the interaction between a unit cell and each neighbor, and neglects interactions between different perturbations. This treatment is exact if Schrieffer-Wolff transformation is truncated to the first (linear) term in its series expansion, but real systems will have an error due to the finite coupling strength. In this section, we describe how we partially compensate for higher-order errors by performing an optimization in a larger system consisting of multiple coupled unit cells (Figure S5a) subject to continuity boundary conditions, within the context of the zero group velocity material.

As an example, we consider a finite element model consisting of two unit cells of the zero group velocity material, where each unit cell is made of two plates (Fig. 3c). We use Comsol Multiphysics to determine the system's eigenmodes and eigenfrequencies at our frequency of interest. Since the system consists of four plates, and each plate contains two modes in that frequency range (Fig S5b), the problem requires the computation of eight eigenmodes of the coupled structure. We then determine the coupling matrix between local modes by utilizing the same procedure as in the case with two plates: We first express the coupled eigenmodes in terms of our local basis (Fig S5b), by probing the displacement field over the test area of each plate (Fig. 1c) and identifying the linear combination of the basis modes that provides the best least-square approximation of the displacement field in the test area (using a Moore-Penrose pseudoinverse). Then we combine the eigenfrequencies and eigenmodes in the local basis representation to determine the reduced-order coupling matrix V^R for the system.

To minimize the error in the system's reduced dynamical matrix (Fig S4c), we utilize a gradient-based method. We parameterize our geometry by allowing the beam locations, thicknesses and angles, as well as the hole locations and radii to change. We then determine the coupling matrix for the original system and for modified systems where we introduce a small change (0.03 mm) in each of the system's parameters. This allows us to assemble a Jacobian matrix J that relates small changes in the geometry to small changes in the coupling matrix. The direction of maximum error descent is given by $\vec{g} = -\left(\vec{k} - \vec{k}_T\right)^T J$, where $\vec{k}$ is a 64-components column vector containing the elements of the coupling matrix V^R, while $\vec{k}_T$ contains the elements of the target matrix. We then identify the optimal amount of change in the direction of $\vec{g}$ by minimizing $\left|\vec{k} + J\alpha\vec{g} - \vec{k}_T\right|$ with respect to α. We then apply this change in the model and recompute the error. Since the Jacobian matrix does not change significantly between gradient iterations, we evaluate it only once at the beginning of the optimization process. Due to the presence of long-range interactions, the optimization algorithm is not able to completely match the system's dynamical matrix V^R to the objective mass-spring model K_{Target} (Fig S5d). This additional optimization step greatly improves the agreement between the metamaterial's response and the target model, reducing the root mean square error in the dispersion relation fourfold from 20.4 Hz (Fig S5e) to 5.1 Hz (Fig S5f).

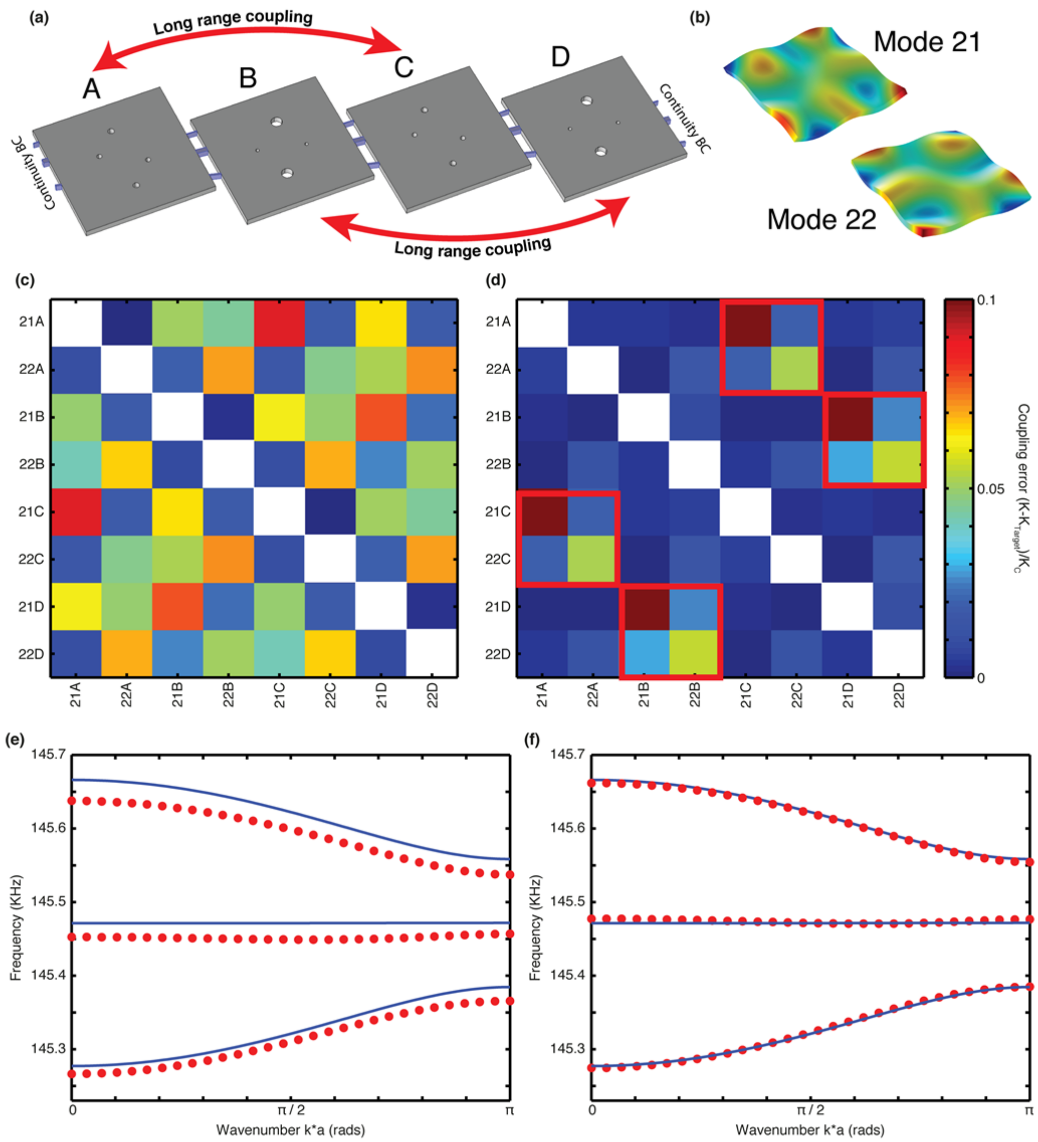

Figure S5 | Higher-order error compensation. a. Finite element model used in the coupled optimization scheme. The model consists of four plates (2 unit cells) subject to continuity boundary conditions. **b.** Eigenmode basis used to describe the displacement of the coupled plates. The eigenmodes correspond to a free plate. **c.** Magnitude of the error between the objective inter-modal coupling stiffnesses and the coupling stiffnesses determined from the finite element model in panel **a**. **d.** Magnitude of the coupling error after the optimization. The red squares indicate long-range interactions. **e.** Band structure of the lattice before the optimization. **f.** Band structure of the lattice after the optimization. In **e** and **f** the blue lines are the analytical predictions from the objective mass-spring model and the red dots correspond to the finite element simulation on the designed physical system.

SI4. Topological Insulator Evaluation

To evaluate the behavior of the designed topological insulator metamaterial, we compare its modal properties to those of the mass-spring model. The eigenfrequency analysis of the physical system agrees well with the mass-spring analytical model (Fig. S6a), and shows two bulk band gaps. This is confirmed by calculating the localization of each mode, defined as its strain energy summed over the unit cells on the edge, normalized by the total strain energy of the mode over the entire finite metamaterial. The localization of both the mass-spring model and designed metamaterial show almost complete localization on the boundary unit cells within the two bands identified in the eigenfrequency analysis. An example mode within the first bulk band gap of the mass-spring model clearly shows the edge mode (Fig. S6b). Figure S7 shows four other example modes within both bulk band gaps in the physical system. The designed topological insulator metamaterial overall shows excellent agreement with the behavior of the corresponding mass-spring model.

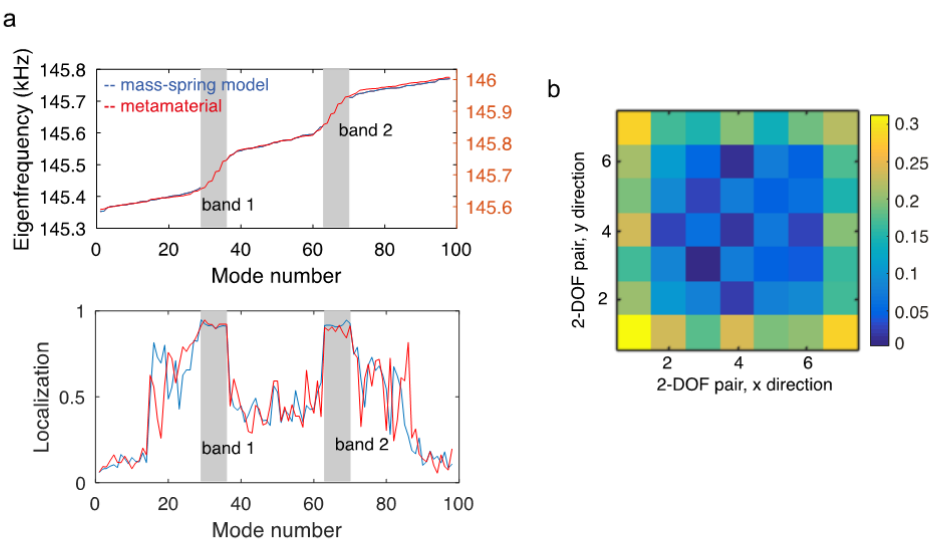

Figure S6 | Topological insulator mass-spring model compared to metamaterial. a. Eigenfrequency analysis and energy localization of mass-spring model compared to the designed metamaterial, both showing two bands of topologically protected edge modes. **b.** Topologically protected edge mode of mass-spring model from Fig. 4a, within band 1. The same mode number is shown in the metamaterial results in Fig. 4d. Each pixel corresponds to a pair of degenerate modes.

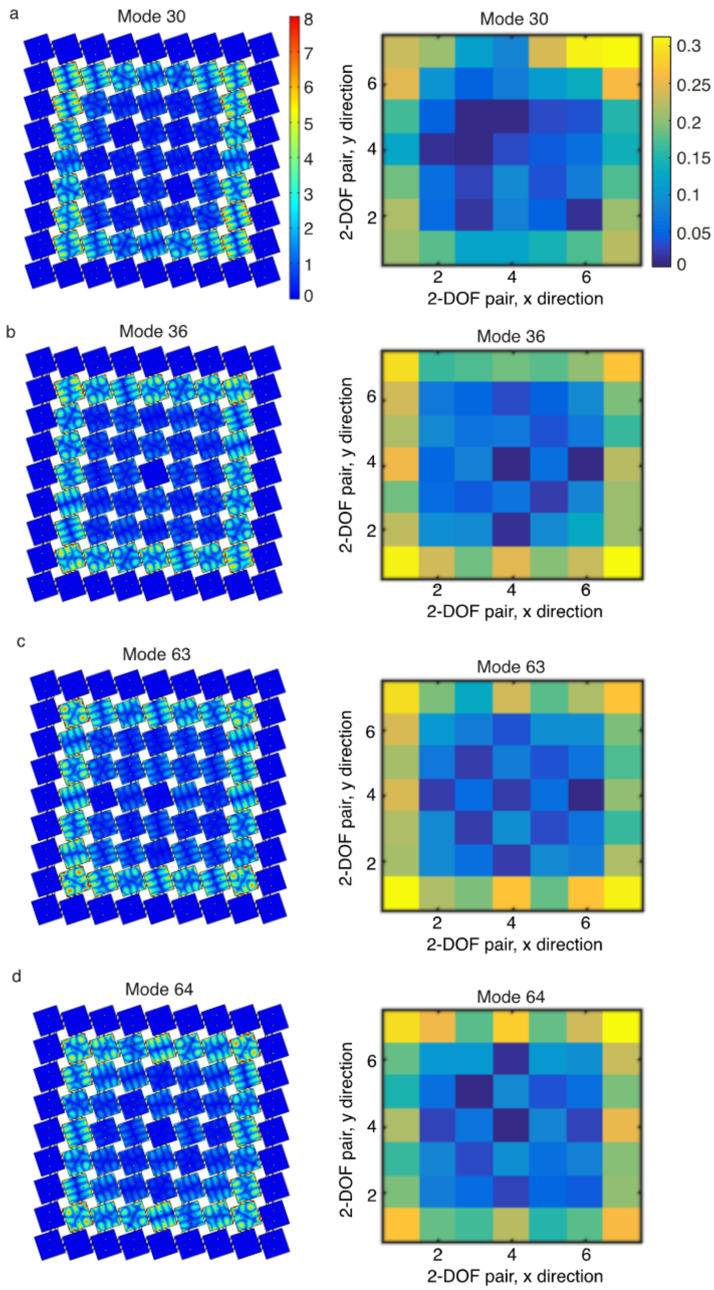

Figure S7 | Four examples of topologically protected edge modes of the designed metamaterial (left) and mass-spring model (right). **a.** Mode 30 and **b.** mode 36 are within the first topologically protected band, and **c.** mode 63 and **d.** mode 64 are within the second topologically protected band. The color bars shown in **a** apply to all plots, and are shown in arbitrary units of modal displacements.